Bidentate ligand modification strategy on supported Ni nanoparticles for photocatalytic selective hydrogenation of alkynes

Jie Wang[1,5,+], Mengxia Wang[4,+], Linjuan Pei[1,5,+], Xianmo Gu[1], Xincheng Li[1,5], Peng Kong[1], Ruiyi Wang[1]*, Xuebin Ke[3]*, Guangtao Yu[2,6]*, and Zhanfeng Zheng[1,5]*

[1]State Key Laboratory of Coal Conversion, Institute of Coal Chemistry, Taiyuan 030001, China
[2]Engineering Research Center of Industrial Biocatalysis, Fujian Province University, Fujian Provincial Key Laboratory of Advanced Materials Oriented Chemical Engineering, College of Chemistry and Materials Science, Fujian Normal University, Fuzhou 350007, China
[3]Department of Chemical Engineering, University of Hull, HU6 7RX, United Kingdom
[4]Laboratory of Theoretical and Computational Chemistry, Institute of Theoretical Chemistry Jilin University, Changchun 130023, China
[5]Center of Materials Science and Optoelectronics Engineering, University of Chinese Academy of Sciences, Beijing 100049, China
[6]Fujian Provincial Key Laboratory of Theoretical and Computational Chemistry, Xiamen University, Xiamen, 361005, China
+These authors contributed equally: Jie Wang, Mengxia Wang, and Linjuan Pei.
*Email: wangruiyi@sxicc.ac.cn; x.ke@hull.ac.uk; yugt@fjnu.edu.cn; zfzheng@sxicc.ac.cn

ABSTRACT:

The design of selective and stable non-precious metal catalysts for hydrogenation of alkyne is highly desirable. In this study, L-lysine modification strategy is applied to support Ni nanoparticles, which greatly improves the stability and photocatalytic performance in the hydrogenation of phenylacetylene to styrene. After modification, the selectivity of styrene increases from 7.2% to 95.8% without apparent activity loss after 4 successive cycles. The adsorption of phenylacetylene on Ni surface are studied by XPS and DFT calculation and a rational reaction mechanism has been proposed. The robust stability is attributed to that both amino and carboxyl groups of L-lysine can function simultaneously as the anchor, much stronger than a single group, to strongly interact with metallic Ni via N and O coordination. The high selectivity to styrene is due to that L-lysine modification results in a larger adsorption energy difference between styrene and phenylacetylene on the surface of Ni, therefore phenylacetylene is preferentially adsorbed on Ni surface. Light irradiation can accelerate the hydrogenation process because that H_2 can be easily activated on Ni surface with the aid of energetic charges from the localized surface plasmon resonance (LSPR) effect of metallic Ni nanoparticles. This protocol shows that the modulation of interaction between ligands and Ni is favorable to design stable, active and selective catalysts for hydrogenation of alkynes.

Keywords: Ni nanoparticles • LSPR • surface L-lysine • phenylacetylene hydrogenation • high selectivity and stability

1. INTRODUCTION

The selective hydrogenation of alkyne to olefin is an important reaction in industry due to its application in pharmaceuticals, agrochemicals, fragrances, polymerization, olefin metathesis reactions and removal of trace alkyne impurities in olefin polymerization industry.[1-6] It is still a great challenge to develop effective catalysts with high catalytic activity and olefin selectivity.[7-8] At present, although Pd and Pt-based catalysts are the most promising ones which show obvious advantages of high olefin selectivity,[9-11] the limited resources and high cost limit their practical applications to some extent. Hence, the development of non-precious metal catalysts like earth abundant Ni provides a low-cost solution for selective hydrogenation of alkyne to olefin.

Ni-based catalysts are widely used in the hydrogenation of alkynes due to its high hydrogenation activity, but still suffer from low olefin selectivity.[12-19] A major reason for low olefin selectivity is the strong adsorption capacity of olefins on the surface of Ni. Strategies including alloying, incorporation of *p*-block elements into interstitial sites of Ni and selective coordination with some amino compounds have been attempted.[20-24] For example, the NiGa intermetallic catalysts with completely isolated Ni sites exhibit high ethylene selectivity, which is ascribed to the preferential acetylene adsorption and enhanced ethylene desorption on the surface of Ni sites.[21] Over-hydrogenation of alkynes can also be suppressed by nickel nitride (Ni_3N) via weak interaction between the alkene product and the Ni_3N active sites.[24] Amino compounds have been used as additives in the phenylacetylene hydrogenation reaction system, which can coordinate with Ni-based catalysts to weaken adsorption of olefins to regulate the hydrogenation of alkynes to olefins.[25-27] It is revealed that the additive *n*-butyl amine with single amino group can increase the alkene selectivity over Ni_1Fe_3 catalyst while facing the difficulty of products separation.[27] Meanwhile, poor stability is also shown over Ni nanoparticles (NPs) modified by imidazolium-amidinate ligands to modulate alkene selectivity.[26] As a consequence, the interaction between single amino compounds and the Ni NPs should be enhanced to fulfil the need of development of an inexpensive, stable, and higher selective Ni-based catalyst in industry and academia.

Recently, it is reported that photoexcited electrons of Ni NPs, due to localized surface plasmon resonance (LSPR) effect under visible light irradiation, can promote catalytic activity and make the reactions proceed at relatively low temperatures.[28-29] Therefore, it is very attractive to drive hydrogenation reaction with solar energy in view of the gradual depletion of fossil resources. This provides a possibility that the activity for phenylacetylene hydrogenation can also be promoted by the LSPR effect of Ni NPs.

Herein, we design an L-lysine (with bidentate ligand, both carboxy and amino groups) modified photocatalyst, i.e. L-lysine modified Ni/Nb_2O_5 (L-lysine/Ni/Nb_2O_5), for photocatalytic hydrogenation of phenylacetylene. Here, Nb_2O_5, a wide band gap semiconductor (~3.2 eV) and irresponsive for visible light ($\geq$ 420 nm),[30] is beneficial to study the photocatalytic properties promoted by the LSPR effect of metal Ni NPs under visible light irradiation. L-lysine/Ni/Nb_2O_5 can achieve high conversion of phenylacetylene while maintaining a high styrene selectivity and can be used for several times with a good stability. The high selectivity of styrene is mainly because styrene has lower adsorption energy on the surface of metallic Ni sites than that of phenylacetylene. The improved stability of Ni-based catalysts is attributed to the strong co-interaction between bidentate ligand of L-lysine and Ni/Nb_2O_5.

2. EXPERIMENTAL SECTION

2.1 Chemicals

Niobium pentoxide (Nb_2O_5, ≥99.99%), nickel nitrate hexahydrate ($Ni(NO_3)_2·6H_2O$), L-lysine and styrene were purchased from Sinopharm Chemical Reagent Co. Ltd and used without further purification. Hydrochloric acid (HCl, 36～38%) and Sodium hydroxide (NaOH) was purchased from Tianjin Kemiou Chemical Reagent Co. Ltd. Phenylacetylene was purchased from Aladdin.

2.2 Preparation of Ni-niobate (10 wt.%Ni)

0.3 g of H-niobate, which was obtained according to previous report,[30-32] and 0.1651 g of $Ni(NO_3)_2·6H_2O$ were put into 50 mL of 0.04 M L-lysine aqueous solution. The obtained mixture was placed in a teflon-lined, sealed with stainless-steel vessel with an inner volume of 100 mL, and then maintained for 24 h at 180 °C. The product was washed with ultrapure water and dried at 80 °C for 12 h and labelled as Ni-niobate.

2.3 Preparation of Ni/Nb_2O_5, $NiO/Ni/Nb_2O_5$ and NiO/Nb_2O_5

For a typical synthesis of 10 wt.%Ni/Nb_2O_5, the prepared Ni-niobate was reduced at 600 °C for 3 h by H_2 (10 mL min^{-1}) in tube furnace to obtain final Ni/Nb_2O_5. Other loadings of Ni NPs were also prepared by the similar method with addition of different amounts of $Ni(NO_3)_2·6H_2O$ in the preparation of Ni-niobate. To obtain $NiO/Ni/Nb_2O_5$ or NiO/Nb_2O_5 having identical Ni loadings with 10 wt.%Ni/Nb_2O_5, above 10 wt.%Ni/Nb_2O_5 was annealed in Air at 200 °C for 2 h and 500 °C 2 h, respectively. Unless otherwise specified, the Ni/Nb_2O_5 below represents 10 wt.%Ni/Nb_2O_5.

2.4 Preparation of L-lysine/Ni/Nb_2O_5

The preparation of Ni/Nb_2O_5 modified with L-lysine is mainly as follows: 0.1 g of Ni/Nb_2O_5 and different qualities of L-lysine (0.0025 g, 0.005 g, 0.01 g, and 0.02 g,) are ground uniformly in an agate mortar, and the uniformly mixture is maintained for 3 h at 200 °C in a tube furnace with H_2 atmosphere to obtain the target catalyst. The mass ratios of L-lysine and Ni/Nb_2O_5 are 0.025, 0.05, 0.1 and 0.02, respectively.

2.5 Adsorption of *n*-hexanoic acid or *n*-hexylamine on the surface of Ni/Nb_2O_5

0.01 g of Ni/Nb_2O_5 and 0.1 mmol of *n*-hexanoic acid or *n*-hexylamine is added in 1 mL of isopropyl alcohol. The obtained mixture is ultrasonically dispersed and dried in a vacuum oven at 80 °C for 12 h. The samples are then characterized by FT-IR and XPS.

2.6 Characterizations

The XRD patterns were tested on a MiniFlex II diffractometer with the conditions of Cu-Kα radiation (λ = 1.5418 Å) and manipulated in a 2θ range of 5-80° at a scanning rate of 8° min^{-1}. The scanning electron microscopy (SEM) images with different multiples were acquired through a JSM-7001F instrument. For the more detailed surface messages, the transmission electron microscopy (TEM) carried out on a JEM-2100F microscope with accelerating voltage of 200 kV was used to characterize the obtained samples. To investigate components and the valence state of elements of catalysts, X-ray photoelectron spectroscopy (XPS) was conducted on a Thermo ESCALAB 250 spectrometer at room temperature using an Al Ka X-ray source ($h\nu$ = 1486.6 eV). The C 1s peak at 284.6 eV was used as a reference for the calibration of the binding energy scale. To investigate the light adsorption behavior of the samples, the UV-Vis diffuse reflectance (UV-Vis-DR) spectra were measured using a Hitachi U-3900 spectrometer. *In situ* diffuse reflectance infrared Fourier transform spectroscopy (DRIFTs) was used to observe the substrates and intermediates adsorption on the surface of catalysts. The total Ni loadings of various based-Ni catalysts were determined by an inductively coupled plasma (ICP) spectrometer on a Thermo iCAP6300 instrument. Thermogravimetric/differential thermal (TG/DTA) analysis was carried out

on a Rigaku TG in N_2 with a heating rate of 10 °C min^{-1}. ^1H and ^{13}C NMR spectroscopy was recorded by Bruker AVANCE IIITM spectrometer (frequencies of 400 and 100 MHz) and the chemical shift was referenced to TMS (tetramethylsilane) by using D_2O as the solvent.

2.7 Photocatalytic phenylacetylene hydrogenation to styrene

Classically, 10 mg of catalyst and 2 mL of phenylacetylene in isopropyl alcohol solution (0.05 M) were added into a 10 mL vial. The vial was then purged with H_2 for 1 min to maintain the H_2 pressure at 1 atm and kept it at 80 °C in an oil bath for 6 h under visible light irradiation (white LED, 600 mW cm^{-2}). After that, the catalyst was filtered with a 0.22 mm nylon syringe filter and the products were analyzed using a Shimadzu 2014C gas chromatography equipped with a WondaCap 5 column. The amount of products and reactants was calculated using an external standard method. The calculation formula for conversion and selectivity is as follows [n(mol), amount of substance].

Conversion = $[n_{(product\ 1)}+n_{(product\ 2)}....]/n_{(reactant)} \times 100\%$

Selectivity = $[n_{(product)}/(n_{(product\ 1)}+n_{(product\ 2)}....)] \times 100\%$.

2.8 Computation details

Based on the density functional theory (DFT), all of the computations are performed by employing the generalized gradient approximation (GGA)[33] with the Perdew-Burke-Ernzerhof exchange-correlation functional within the frame of Vienna *ab initio* simulation package (VASP).[34-35] A 400-eV cutoff is employed for the plane-wave basis set. A semi-empirical van der Waals (vdW) correction is used to account for the dispersion interactions,[36] and the projector-augmented plane wave (PAW) is used to describe the electron-ion interactions.[37-38] The geometrical optimization of bulk Ni structure is carried out using 7×7×7 Monkhorst-Pack grid *k*-points. Based on the optimized 3D structure, we simulated the Ni(111) surface by the slab with three atomic layers. For all the studied slab systems, 3×3×1 *k*-points are adopted for the structural optimizations, where the two atomic layers below are frozen and the remaining atoms are relaxed during the calculation process. For all computations, the convergence threshold is set as 10^{-4} eV in energy.

Moreover, the adsorption energy involved in this work can be computed by the following equation:

$\Delta E_{ads} = E_{slab} + E_X - E_{total}$

where E_{total} and E_{slab} are the total energies of the studied system with and without the adsorbate, and E_X is the energy of adsorbed molecule.

3. RESULTS AND DISCUSSION

3.1 Structure analysis and selective hydrogenation performance of L-lysine modified Ni/Nb_2O_5

The typical preparation process of L-$lysine_x/Ni/Nb_2O_5$ (*x* is the corresponding mass ratio of L-lysine and Ni/Nb_2O_5) catalyst is shown in Figure 1a. Nb_2O_5 exhibits a fibril morphology as observed from the SEM image (Figure 1b). The SEM and TEM images of classical L-$lysine_{0.05}/Ni/Nb_2O_5$ show that Ni NPs with an average particle size of 31.5 nm are uniformly distributed on the surface of the Nb_2O_5 fiber (Figure S1). The HRTEM image shown in Figure 1c proves the existence of Ni(111) plane with a *d*-spacing of 0.203 nm. The EDX elementary mapping shows that the N element of L-lysine is uniformly distributed on the surface of Ni/Nb_2O_5 besides Ni, Nb and O elements of L-$lysine_{0.05}/Ni/Nb_2O_5$. The existing form of L-lysine on the catalyst is characterized by Fourier transform infrared spectra (FT-IR) analysis (shown in the next

section). The XRD diffraction peaks of Ni/Nb_2O_5 modified with different amounts of L-lysine molecules all show the mixture of metallic Ni (JCPDS no. 87-0712) and Nb_2O_5 (JCPDS no. 28-0317). And the diffraction peaks of metallic Ni exhibit no obvious change with the increase of the starting material L-lysine compared with that of the original Ni/Nb_2O_5 (Figure 1d), suggesting that L-lysine modification strategy cannot affect the crystal structure of Ni NPs on the surface of Nb_2O_5.

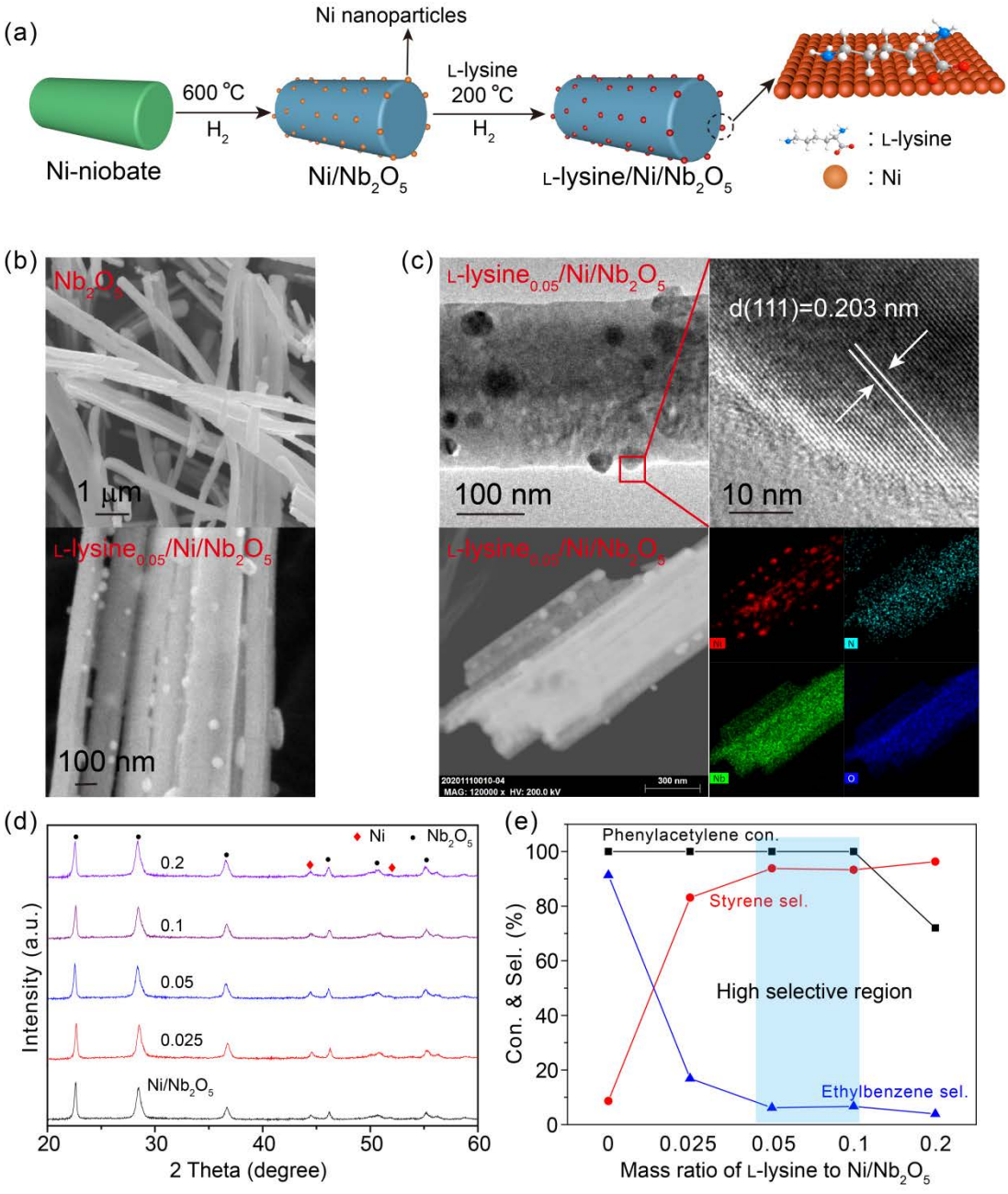

Figure 1 Synthesis, characterization and photocatalytic performance of L-lysine modified Ni/Nb_2O_5. (a) Schematic diagram showing the preparation of L-lysine modified Ni/Nb_2O_5. (b) SEM images of Nb_2O_5 and L-$lysine_{0.05}/Ni/Nb_2O_5$. (c) TEM, HRTEM, STEM and elementary mapping images of L-$lysine_{0.05}/Ni/Nb_2O_5$. (d) XRD patterns of L-lysine/Ni/Nb_2O_5 with different

mass ratio of L-lysine to Ni/Nb_2O_5. (e) Influence of mass ratio of L-lysine to Ni/Nb_2O_5 on phenylacetylene hydrogenation. Reaction conditions: photocatalyst, 10 mg; temperature, 80 °C; time, 12 h; isopropyl alcohol, 2 mL; phenylacetylene, 0.1 mmol; H_2, 1 atm; white LED, 600 mW cm^{-2}.

The photocatalytic performance of various catalysts in phenylacetylene hydrogenation reaction are studied. It is obvious that L-lysine modification strategy can remarkably increase styrene selectivity with the increase of the mass ratio of L-lysine to Ni/Nb_2O_5 (Figure 1e). Ni/Nb_2O_5 without L-lysine modification shows low styrene selectivity (7.2%, Table 1, entry 1) with >99.9% of phenylacetylene conversion. The styrene selectivity can be increased to 95.8% at full conversion of phenylacetylene when the mass ratio of L-lysine to Ni/Nb_2O_5 is 0.05 (Table 1, entry 2). This ratio is fixed if no specific definition. However, excess L-lysine molecules can surpress the conversion of phenylacetylene remaining the high styrene selectivity (Figure 1e). This suggests the importance of L-lysine molecules in regulating styrene selectivity over Ni/Nb_2O_5. In the control experiment, the hydrogenation of phenylacetylene has been carried out over Ni/Nb_2O_5 catalyst modified with *n*-hexylamine, *n*-hexanoic acid and 1-aminohexanoic acid, respectively (Table 1, entries 3-5). It can be clearly found that both *n*-hexylamine and 1-aminohexanoic acid can regulate hydrogenation of phenylacetylene to styrene. However, the addition of *n*-hexanoic acid hardly modulate the selectivity of styrene and affect the conversion of phenylacetylene. These results indicate that there is no work to modulate the selectivity of styrene for carboxyl groups of L-lysine, while amino group of L-lysine mainly interact with metallic Ni to modulate selectivity of styrene.

3.2 Bidentate ligand in L-lysine co-anchoring on Ni towards simultaneously enhanced stability

In the control experiment, the photocatalytic stability of Ni/Nb_2O_5 adsorbing *n*-hexylamine molecules [Ni/Nb_2O_5(*n*-hexylamine)] and L-$lysine_{0.05}/Ni/Nb_2O_5$ are evaluated (Figure 2a-c). It is shown that Ni/Nb_2O_5(*n*-hexylamine) exhibits poor stability (Figure 2a). But high stability is observed for L-$lysine_{0.05}/Ni/Nb_2O_5$ (Figure 2b).The XRD pattern of recycled L-$lysine_{0.05}/Ni/Nb_2O_5$ has no obvious change compared to that of fresh L-$lysine_{0.05}/Ni/Nb_2O_5$ (Figure S2). Meanwhile, the FT-IR characteristic peaks of L-lysine are well preserved for the recycled L-$lysine_{0.05}/Ni/Nb_2O_5$ (Figure 2c, the recognition of L-lysine molecules will be discussed in the following paragraph). These results indicate that L-$lysine_{0.05}/Ni/Nb_2O_5$ is effective and stable photocatalyst for selective hydrogenation of phenylacetylene to styrene.

The recognition of L-lysine molecules on the surface of Ni/Nb_2O_5 and the strong interaction between L-lysine molecules and Ni/Nb_2O_5 is proved by FT-IR in Figure 2d. The $–NH_3^+$ asymmetric bending vibration peak at 1630 cm^{-1}, the $–COO^–$ asymmetric stretching vibration peak at 1580 cm^{-1} and the $–COO^–$ symmetric stretching vibration peak at 1408 cm^{-1} are shown,[39] impling that the pristine L-lysine molecules are mainly in the zwitterionic form. It can be clearly found that the asymmetric stretching peak of $–NH_3^+$ shifts from 1630 to 1623 cm^{-1} and a new asymmetric stretching peak of $–NH_2$ appears at 1597 cm^{-1}, when the mass ratio of L-lysine and Ni/Nb_2O_5 is 0.025.[39-40] At the same time, the symmetric stretching vibration peak of $–COO^–$ shifts from 1408 to 1404 cm^{-1} and there is no appearance for asymmetric stretching vibration peak of $–COO^–$. This can be ascribed to the terminal amine group of L-lyisne, which is reorientated because

of the influence of temperature and the zwitterionic form of L-lysine is also retained due to high coverage of L-lysine.[39] When further increasing mass ratio to 0.2, the characteristic peaks of $–NH_3^+$, $–NH_2$ and $–COO^–$ shifts from 1623 to 1617 cm^{-1}, 1597 to 1590 cm^{-1} and 1404 to 1400 cm^{-1}, respectively. Meanwhile, when the mass tatio is 0.2, the relative strength of asymmetric bending peak of $–NH_3^+$ almost disappears while the asymmetrical stretching vibration peak of $–NH_2$ and asymmetrical stretching vibration peak of $–COO^–$ are mainly displayed. These results illustrate that the interaction between $–NH_2$ and $–COO^–$ groups of L-lysine and Ni/Nb_2O_5 is dominant with the increase of mass ratio of L-lysine and Ni/Nb_2O_5, while the interaction between $–NH_3^+$ and $–COO^–$ of L-lyisne and Ni/Nb_2O_5 is also present.

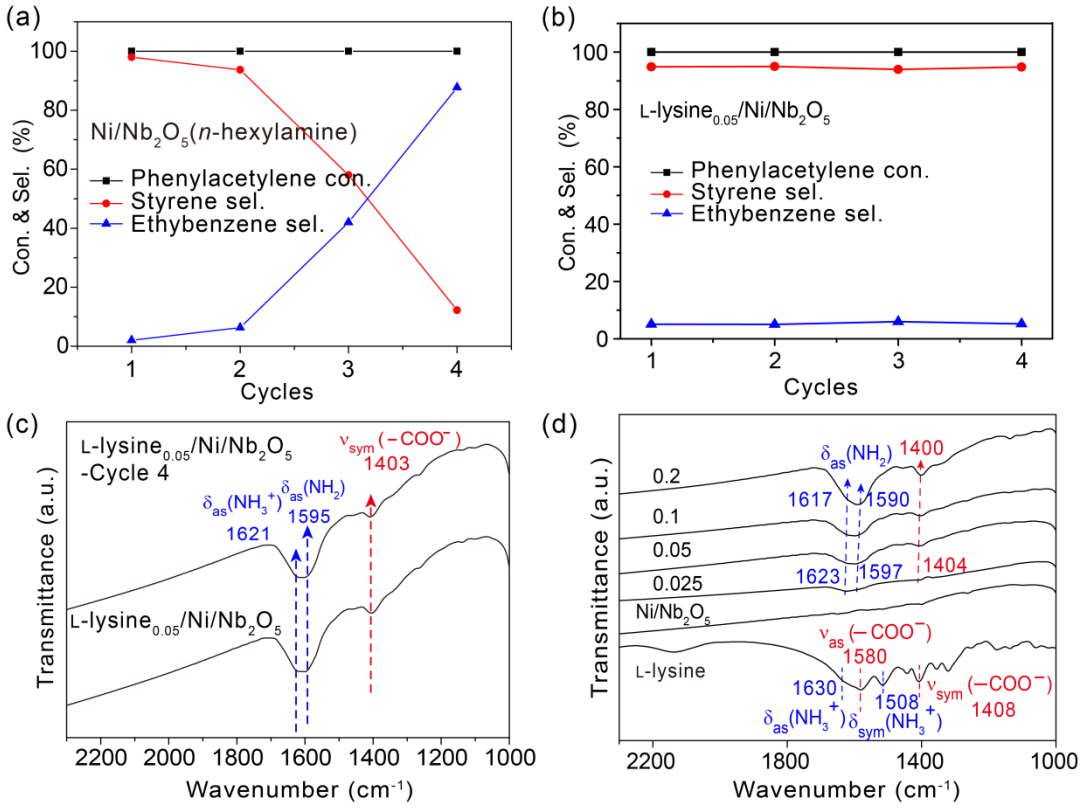

Figure 2 Recognition of L-lysine molecules adsorption and stability on the surface of Ni/Nb_2O_5. (a) FT-IR spectra of Ni/Nb_2O_5 and L-lysine/Ni/Nb_2O_5 with different mass ratio of L-lysine and Ni/Nb_2O_5. The photocatalytic stability of (b) Ni/Nb_2O_5(*n*-hexylamine) and (c) L-$lysine_{0.05}/Ni/Nb_2O_5$ in four cycles. Reaction conditions: phenylacetylene, 0.1 mmol; photocatalyst, 10 mg; isopropyl alcohol 2 mL; H_2, 1 atm; temperature, 80 °C; white LED, 600 mW cm^{-2}; 6 h. (d) FT-IR spectra of L-$lysine_{0.05}/Ni/Nb_2O_5$ before and after reaction.

The strong interaction between Ni/Nb_2O_5 and L-lysine molecules is further confirmed by XPS analysis (Figure S3a-e). Compared with the binding energy at 852.6 eV of metallic Ni of the original Ni/Nb_2O_5,[15, 41-44] the binding energies of metallic Ni $2p_{3/2}$ of Ni/Nb_2O_5 modified with different amounts of L-lysine gradually shift from 852.3 to 851.6 eV (Figure S3a), implying that L-lysine molecules have strong interaction with Ni/Nb_2O_5, leading to more enriched electrons

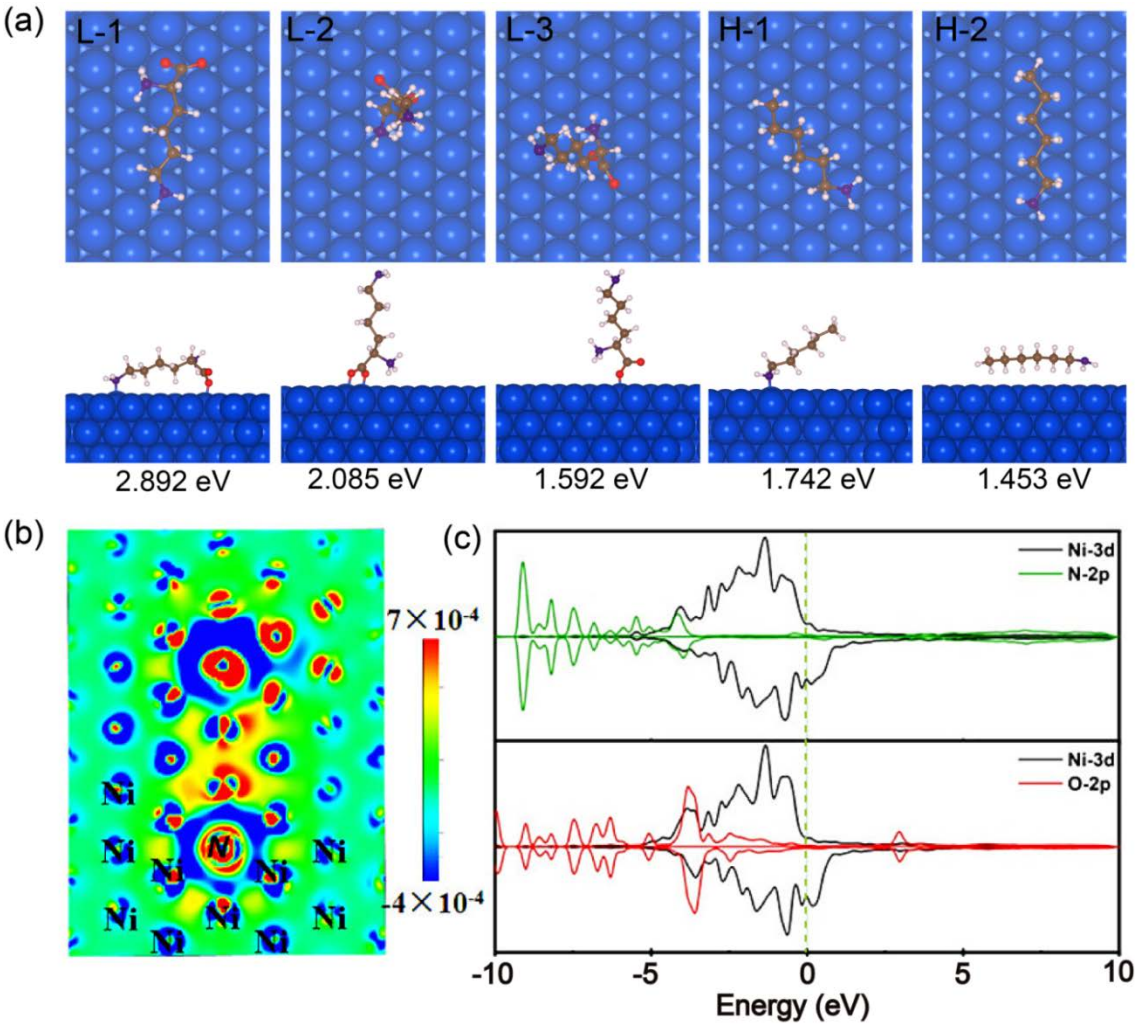

Figure 3 Adsorption mode of L-lysine (bidentate ligand) and *n*-hexylamine (monodentate ligand) on the surface of metallic Ni. (a) Top and side views of the optimized structures with L-lysine (L-1 ~ L-3) and *n*-hexylamine (H-1 and H-2) on the different adsorption positions of Ni(111) surface. Red ball, O; grey ball, H; brown ball, C; blue ball, N. (b) The charge density difference ($\Delta\rho$) for L-1 structure, where the blue and red areas mean that the electron density decreases and increases, respectively. (c) Partial density of states (PDOS) for L-1 structure.

around metallic Ni. At the same time, the corresponding binding energies of Nb $3d_{3/2}$ and $3d_{5/2}$ migrated from 210.1 to 209.4 eV and 207.3 to 206.6 eV (Figure S3b),[32] respectively, confirming that L-lysine molecules also can interact with Nb_2O_5 (also demostrated in Figure S4) and make electrons around Nb more enriched. Correspondingly, the binding energy of O 1s of –C=O decreases from 531.6 to 531.1 eV (Figure S3c), the binding energy of N 1s of –NH gradually decreases from 399.8 eV to 399.4 eV (Figure S3d), the binding energy of C 1s of –C=O decreases from 288.6 to 287.8 eV, and the binding energy of C 1s of C–N increases from 285.4 to 285.8 eV (Figure S3e). This is because the electrons around metallic Ni transfer to the N and O of L-lysine (also demonstrated in Figure 3b) while the high density electrons of inner *s* or *p* orbitals around Ni migrate to the outer 2*p* orbital of Ni,[32] leading to co-increasing of binding energies of O 1*s* and N 1*s* of L-lysine and Ni $2p_{3/2}$ of metallic Ni. Meanwhile, the increase of the binding energies of the corresponding C connected to the $–COO^–$ and –NH groups is mainly because the $–COO^–$ and –NH

of L-lysine can attract surrounding electrons of C. This result combined with that of FT-IR confirms that there is a strong interaction between Ni NPs and the $–COO^-$ and $–NH_2$ or $–NH_3^+$ groups of the L-lysine molecules.

To figure out the adsorption mode of L-lysine on the metallic Ni as the active center, various adsorption modes of L-lysine molecule on the surface of metallic Ni are optimized and corresponding adsorption energies are calculated by considering possible spatial conformations (Figure 3a). The computed results reveal that a total of three configurations can be achieved (Figure 3a), among which the configuration L-1 can exhibit the largest adsorption energy (ΔE_{ads} = 2.892 eV), indicating the highest structural stability. For the most sable configuration L-1, the adsorbed L-lysine can lie down the Ni(111) surface, where the N atom in $–NH_2$ group and O atom in $–COO^-$ group are bonded to the Ni atoms on the surface to form the Ni–N and Ni–O chemical bonds at the same time (Figure 3b). The calculated Ni–N and Ni–O bond lengths can be 2.043 and 2.001 Å, respectively. The formation of Ni–N and Ni–O bonds can be also supported by the computed results of partial density of states (PDOS), in which the N- or O-2*p* and Ni-3*d* orbitals have obvious hybridization. Moreover, for the purpose of comparison, the adsorption of the *n*-hexylamine with the similar structure but the chain end modified by only NH_2 group is also considered (Figure 3a). The results show that two adsorption configurations of *n*-hexylamine can be obtained on the Ni(111) surface, where the configuration H-1 (1.742 eV) has larger adsorption energy than the configuration H-2 (1.453 eV), in view of the formation of Ni-N bond. However, the adsorption energy of H-1 (1.742 eV) can be much smaller than that of L-1 (2.892 eV), indicating that L-lysine can be anchored on the Ni(111) surface more effectively, due to the simultaneous existence of both the Ni–N and Ni–O bonds. This result combined with the fact that *n*-hexanoic acid does not affect the activity of the active metal Ni (Table 1, entry 4), suggesting that the strong co-interaction between $–NH_2$ and $–COO^-$ groups of L-lysine and Ni/Nb_2O_5 is favorable to improve stability of L-lysine/Ni/Nb_2O_5, while amino group of L-lysine mainly interact with metallic Ni to modulate selectivity of styrene.[45]

The thermal analysis is conducted to study the thermal stability of L-lysine modified catalyst. The TG and DTA curves of L-lysine show the classic endothermic peak at 226.5 °C attributed to the melting point of L-lysine,[46] confirming that L-lysine molecules are very stable and no polymerization or decomposition occurs at 200 °C (Figure S5a). Meanwhile, the weak endothermic peak at 260.3 °C attributed to the decomposition of L-lysine of L-lysine$_{0.05}$/Ni/Nb_2O_5 is also shown in Figure S5b, demonstrating the stability of L-lysine$_{0.05}$/Ni/Nb_2O_5. ^{1}H NMR spectra of L-lysine molecules before and after heat treatment at 200 °C are shown in Figure S5c. The typical proton signals for –CH and $–CH_2$ are all observed except for that of $–NH_3^+$ and $–NH_2$ group because of the fast deuterium exchange in D_2O solvent.[46] The changes for CH_2 for the L-lysine heat-treated at 200 °C can be caused by hydrogen bonds between the terminal amino groups of L-lysine molecules.[39] Hence, the L-lysine molecules can be stably present on the surface of Ni/Nb_2O_5 at 200 °C.

In order to study the effect of preparation temperature on the interaction between L-lysine and Ni/Nb_2O_5, FI-IR spectra of L-lysine$_{0.05}$/Ni/Nb_2O_5 prepared at different temperatures are shown in Figure S5d. It can be found that the characteristic peaks of the pristine L-lysine are only displayed at room temperature. The characteristic peaks of the $–NH_3^+$ and $–COO^-$ groups shift significantly when the preparation temperature reaches a higher temperature. New characteristic peak of the $–NH_2$ group at 1596 cm^{-1} appears at 150 °C. When preparation temperature rises to 200 °C, new

characteristic peak of the $–NH_2$ group shifts to lower wavenumber at 1595 cm^{-1}, the characteristic peak of $–NH_3^+$ group decreases to 1621 cm^{-1} and the characteristic peak of $–COO^–$ group shifts to 1403 cm^{-1}. These results indicate that the strong interaction between both $–NH_2$ and $–COO^–$ groups of L-lysine molecules and Ni/Nb_2O_5 can be achieved under high temperature conditions and the strong interaction is mainly dependent on $–NH_3^+$ and $–COO^–$ groups of L-lysine molecules at low temperature. Moreover, L-$lysine_{0.05}/Ni/Nb_2O_5$ with preparation temperature below 200 °C (150 and 25 °C) shows very low conversion of phenylacetylene (Table 1, entries 6 and 7), indicating that high selectivity of styrene at full conversion of phenylacetylene can be achieved when both $–NH_2$ and $–COO^–$ groups of L-lysine interact with Ni/Nb_2O_5.

3.3 Light enhanced H_2 activation over metallic Ni NPs

The relationship between photocatalytic activity and incident light intensity is investigated using L-$lysine_{0.05}/Ni/Nb_2O_5$ to clarify the function of visible light. As shown in Figure S6a, when light intensity increases from 300 to 600 mW cm^{-2}, the light irradiation contribution increases from 44.9% to 76.9%. The kinetics of different temperatures (70, 80 and 90 °C) are also carried out to calculate the activation energies in the presence or absence of light, which is favorable to clarify the increase of photocatalytic performance using L-$lysine_{0.05}/Ni/Nb_2O_5$ catalyst (Figure S7). The reaction rate constants at different temperatures under light or dark conditions are obtained (Figure S7a and S7b). The calculated activation energy of phenylacetylene over L-$lysine_{0.05}/Ni/Nb_2O_5$ under light irradiation is 88.1 kJ mol^{-1} (Figure S7c), which is remarkably lower than that (112.3 kJ mol^{-1}, Figure S7d) in the dark according to the Arrhenius equation.[47] The significant decrease in the activation energy further confirms that light can facilitate conversion of phenylacetylene.

According to the previous report,[48-51] photoexcited metal electrons accelerated reactions mainly through photothermal effect and electron transfer mechanism. Hence, the action spectrum is conducted over L-$lysine_{0.05}/Ni/Nb_2O_5$ (Figure S6b). The strong LSPR effect of metallic Ni NPs is also observed in all L-lysine modified Ni/Nb_2O_5 (Figure S6c).[29, 52] Apparently, the Apparent quantum yield (AQY) values track with the UV-Vis diffuse reflectance spectrum of L-$lysine_{0.05}/Ni/Nb_2O_5$, in which a broad peak centered at about 550 nm is attributed to the typical plasmonic absorption of metallic Ni NPs. This result is consistent with the wavelength-dependent performances over Ni/Al_2O_3 for CO_2 reduction, which is driven from the LSPR effect of Ni NPs.[29] The result suggests that phenylacetylene hydrogenation reaction is predominately driven by photoexcited electrons transfer in virtue of LSPR effect of metallic Ni NPs.

To demonstrate the key role of the metallic Ni NPs, NiO/Nb_2O_5, and $NiO/Ni/Nb_2O_5$ catalysts comprising metallic and/or oxidized Ni are also prepared with Ni-niobate as precursor[32] and demonstrated by XRD, TEM, HRTEM and XPS in Figure S8-12. As detected by inductively coupled plasma mass spectrometry (ICP), the Ni contents of Ni/Nb_2O_5, NiO/Nb_2O_5, and $NiO/Ni/Nb_2O_5$ catalysts are 6.3 wt.%, 6.6 wt.%, and 6.3 wt.% (Table S1, entries 1-3), respectively. And the statistical particle size of Ni NPs for Ni/Nb_2O_5 is about 30.4 nm (Figure S8b). Ni/Nb_2O_5 shows the highest phenylacetylene conversion (>99.9%) with poor styrene selectivity (7.2%) under visible light irradiation at 12 h compared with NiO/Nb_2O_5 and $NiO/Ni/Nb_2O_5$ (Table 1, entries 1 and 8-9), indicating that metallic Ni plays a vital role in the enhancement of photocatalytic performance. The reaction cannot proceed without Ni/Nb_2O_5 both in dark and light, indicating that Ni/Nb_2O_5 photocatalyst is necessary for the selective hydrogenation of phenylacetylene. In addition, as the Ni loading of Nb_2O_5 increases, phenylacetylene conversion gradually increases (Figure S9a-b). The good photocatalytic performances of Ni-based catalysts

with different supports are also shown in Table S3. Commercial Ni power or Ni foam shows poor photocatalytic performance (Table 1, entries 10 and 11), illustrating that it is important that Ni NPs disperses on the surface of supports. These results further demonstrate that metallic Ni is the active center to increase photocatalytic performance for selective hydrogenation of phenylacetylene.

Table 1 Photocatalytic performance of various catalysts for phenylacetylene hydrogenation

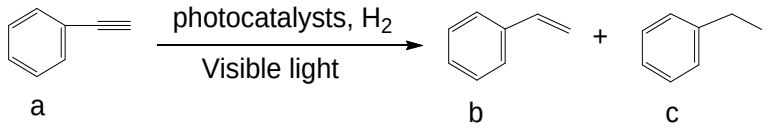

Entry	Catalysts	Con. (%)	Sel. (%)	
			b	c
1	Ni/Nb_2O_5	>99.9	7.2	92.8
2	L-lysine/Ni/Nb_2O_5	>99.9	95.8	4.2
3	Ni/Nb_2O_5(*n*-hexylamine)	>99.9	95.3	4.7
4	Ni/Nb_2O_5(*n*-hexanoic acid)	>99.9	14.5	85.5
5	Ni/Nb_2O_5(1-aminohexanoic acid)	>99.9	94.3	5.7
6	L-lysine/Ni/Nb_2O_5 (150 °C)	7.8	96.9	3.1
7	L-lysine/Ni/Nb_2O_5 (25 °C)	7.4	97.3	2.7
8	$NiO/Ni/Nb_2O_5$	12.1	95.7	4.3
9	NiO/Nb_2O_5	2.0	99.9	n.d.
10	Ni powder	12.2	95.5	4.5
11	Ni foam	4.2	99.9	n.d.
12	Nb_2O_5	n.d.	n.d.	n.d.

Reaction conditions: photocatalysts, 10 mg; temperature, 80 °C; time, 12 h; isopropyl alcohol, 2 mL; phenylacetylene, 0.1 mmol; H_2, 1 atm; white LED, 600 mW cm^{-2}.n.d. = not detected.

There are no phenylacetylene or styrene conversion when reaction is conducted in Ar over Ni/Nb_2O_5 catalyst, indicating the active hydrogen species are ascribed to H_2 rather than isopropyl alcohol. In addition, no reaction occurs over Nb_2O_5 in H_2 atmosphere (Table 1, entry 12). The results suggest that metallic Ni plays a crucial role in activating H_2.

The H_2 activation process is schematically shown and clarified with or without light irradiation using *in situ* DRIFTs in Figure 4a. With time increased from 0 to 140 min, the obvious bands at 2973, 2934 and 2861 cm^{-1} can be assigned to the stretching vibration of $–CH_x$ ascribed to the product of residual CO_2 methanation with H_2 in 80 °C in the dark, indicating that H_2 can be dissociated homolytically on the surface of Ni NPs.[9] However, when H_2 activation experiment is conducted under light irradiation, the intensity of stretching vibration peaks of $–CH_x$ at 30 min is obviously higher than that at 140 min in dark, indicating light can facilitate H_2 activation on the surface of Ni and the production of $–CH_x$ because of the fast methanation process. The results indicate that light can excite electrons of metal Ni by LSPR effect of Ni NPs to induce H_2 activation quickly and then increase the phenylacetylene conversion.

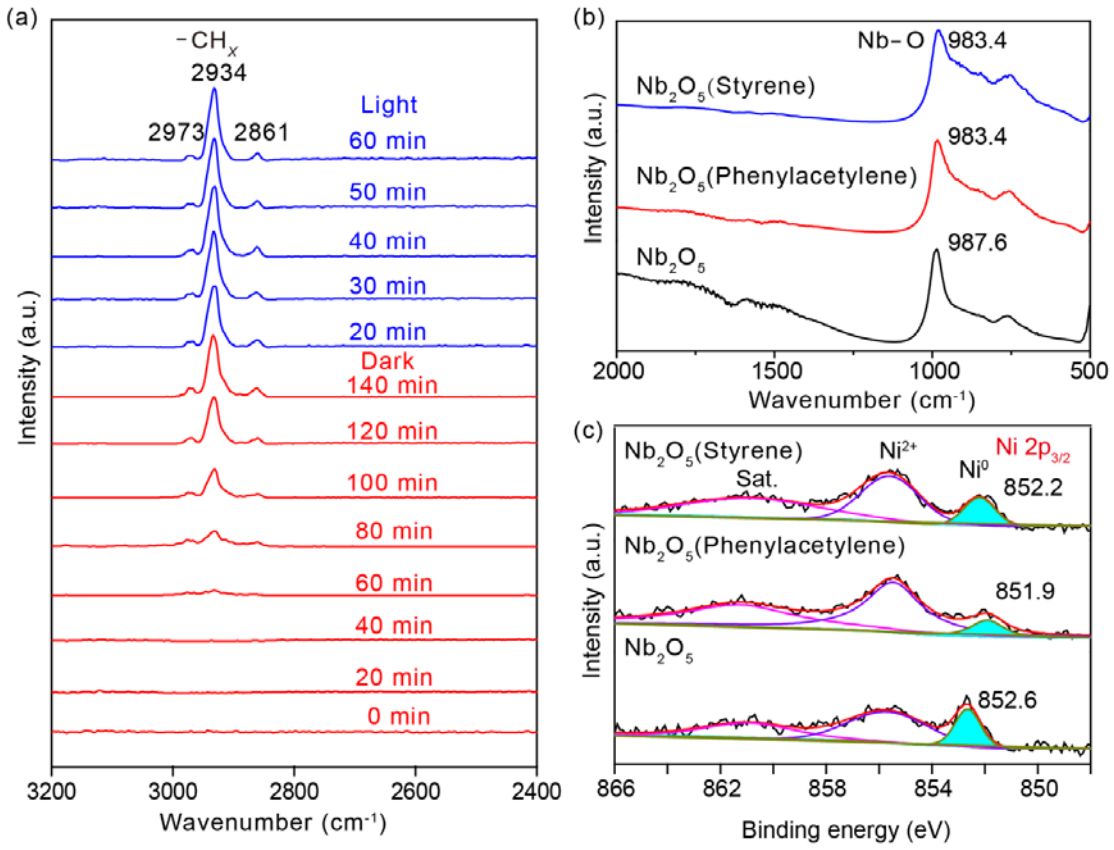

Figure 4 Observation of H_2 activation process and the interaction between phenylacetylene/styrene and catalyst surface. (a) H_2 activation on the surface of L-lysine$_{0.05}$/Ni/Nb_2O_5 in dark and light. (b) DRIFTs of phenylacetylene and styrene adsorbed on Nb_2O_5, respectively. (c) Ni 2*p* XPS spectra of Ni/Nb_2O_5 after phenylacetylene and styrene adsorption, respectively.

3.4 Proposed selective control and reaction mechanism

Because the identical catalytic performance is shown over Ni/Nb_2O_5 and L-lysine$_{0.05}$/Ni/Nb_2O_5 within 6 h in Figure S13, L-lysine molecules of L-lysine$_{0.05}$/Ni/Nb_2O_5 cannot alter the status of preferential activation of phenylacetylene molecules compared with that over Ni/Nb_2O_5. Hence, in order to further study whether metallic Ni or Nb of Ni/Nb_2O_5 is preferential active site of phenylacetylene or styrene hydrogenation, the DRIFTs of two molecules adsorbed on the surface of Nb_2O_5 are shown in Figure 4b. Identical variation of the infrared stretching vibration peak of Nb–O of Nb_2O_5 can be observed when adsorbing the phenylacetylene or styrene, indicating that preferential adsorption and activation of substrate molecules on the surface of Nb_2O_5 is impossible. To investigate the influence of phenylacetylene and styrene on metallic Ni, XPS spectra of Ni/Nb_2O_5(phenylacetylene) and Ni/Nb_2O_5(styrene) are shown in Figure 4c. It can be found that when Ni/Nb_2O_5 absorbs phenylacetylene or styrene, the binding energy of metallic Ni shifts from 852.6 to 851.9 or 852.2 eV, respectively, indicating the strong adsorption between phenylacetylene and metallic Ni, which can be also supported by our DFT calculations. Specifically, the computed results reveal that the styrene can be stably adsorbed on the pure Ni(111) surface with the large adsorption energy as 3.221 eV (I, Figure S14a), where all the C atoms can be alternately located over the top sites of Ni atoms and over the hollow sites Ni-Ni-Ni,

with a distance about 2.000 Å between the molecular and Ni surfaces. Comparatively, when depositing the phenylacetylene on the pure Ni(111) surface (II, Figure S14b), larger adsorption energy (4.078 eV) can be observed, where all six C atoms in benzene ring can also be alternately located at the top sites of Ni atoms and the hollow sites Ni-Ni-Ni with a distance about 1.989 Å between the molecular and Ni surfaces, while the remaining two C atoms in acetylene part lie at the hollow sites Ni-Ni-Ni with a shorter distance of 1.339 Å, indicating the stronger adsorption interaction. The results suggest that a stronger interaction between phenylacetylene and metallic Ni is clarified, which is in accordance with the result that the adsorption energy (1.81 eV) to 1,2-diphenylethyne reactant of Ni(111) is higher than that (0.99 eV) to E-stilbene.[24] Therefore, the metallic Ni active center preferentially activates phenylacetylene molecules in the early stage of photocatalytic reaction, while styrene continues to be activated and hydrogenated in the late stage of the reaction for Ni/Nb_2O_5 catalysts.

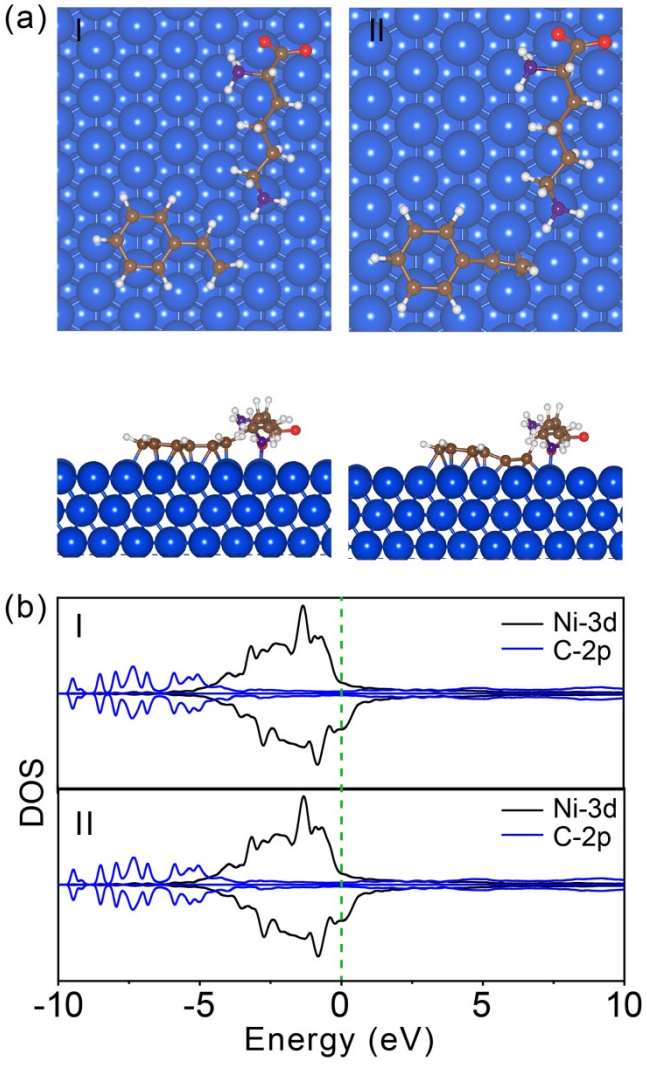

Figure 5 Adsorption of styrene and phenylacetylene near the $-NH_2$ group on the surface of L-lysine modified Ni(111). (a) Top and side views of the optimized structures with styrene (I) and phenylacetylene (II) adsorbed on the L-1 surface, (b) as well as the corresponding partial density of states (PDOSs).

Based on the most stable L-1 structure, we further investigate the adsorptions of styrene and

phenylacetylene on the Ni(111) surface functionalized by L-lysine to reveal the nature that L-lysine can control the selectivity of styrene (Figure 5a). When adsorbing styrene and phenylacetylene near the $-NH_2$ group on the surface of L-lysine modified Ni(111), similar structural features can be observed with that on the surface of pure Ni(111), but the correlative distances between the molecules and Ni surface are longer (about 0.040 Å for the former and 0.033 Å for the latter) than the original distances. As a result, their calculated adsorption energies (2.671 and 3.639 eV, respectively) can become smaller than the corresponding those of pristine Ni(111) surface, but the difference between them increases, which improves the selectivity for styrene. This can be mainly due to the evident electron transfer between the Ni(111) surface and the NH_2 group in L-lysine (Figure 3b), which can effectively modulate the electron density of Ni atoms near the $-NH_2$ group. Moreover, such the large adsorption energies for styrene and phenylacetylene on the L-lysine modified Ni(111) surfaces can be mainly attributed to the effective hybridization between the 2*p* orbitals of correlative C and 3*d* orbitals of Ni atoms, as revealed the computed DOS results (Figure 5b). Overall, employing L-lysine can effectively functionalize the Ni(111) surface, which can be considered as an effective strategy to improve the selectivity of styrene and ensure the high structural stability simultaneously.

The reaction containing styrene is also conducted over Ni/Nb_2O_5 to study the effect of charge density of metallic Ni modulated by styrene on the phenylacetylene hydrogenation reaction, (Figure S15). It can be clearly found that with the increase of styrene content, the phenylacetylene conversion increases firstly and then decreases. According to previous reports,[9, 43] the increased electron density of metallic Ni is more favorable for the activation of H_2 under visible light irradiation, because high electrons density can provide more opportunities to denote *d*-electrons of Ni NPs to the antibonding orbital of H_2 to accelerate homolytic dissociation of H_2. These results suggest that the electrons state of metallic Ni can be modulated by styrene to increase phenylacetylene conversion. This finding provide an novel understanding for the promoted photocatalytic performance of LSPR metal catalysts through *in situ* electronic state modulation.

Based on the above analysis, a plausable mechanism of phenylacetylene hydrogenation on the surface of Ni/Nb_2O_5 modified with L-lysine molecules is proposed. Firstly, the visible light penetrates L-lysine molecules and the hot electrons generated from metal Ni via LSPR effect can make H_2 to be activated and split into Ni–H.[53] Then phenylacetylene adsorbed on the surface of metallic Ni is transformed into styrene by the hydrogenation process. The productive styrene molecules can increase the charge density on the surface of metal Ni, leading to generate more hot electrons to participate in the activation of H_2, thereby enhancing the conversion of phenylacetylene to styrene. Because styrene has longer distance and smaller adsorption energy on the surface of L-lysine modified metallic Ni than that of phenylacetylene, thereby hindering the excessive hydrogenation of styrene, and finally maintaining the high selectivity of styrene.

3.5 Extension of L-lysine modification strategy

The extensional applications of other aromatic alkynes, different supports, different metals and other amino acids modification are summarized in Table S2-S4. The conversion of aromatic alkynes with electron withdrawing groups (–F and –Cl) is much higher than that with electron donating groups ($-CH_3$ and $-NH_2$) in Table S2. There is no exception that more than 90% of aromatic alkenes selectivity for the aromatic alkynes hydrogenation is achieved over L-$lysine_{0.05}/Ni/Nb_2O_5$ whether the reaction is conducted with or without light irradiation. These results demonstrate that the aromatic alkynes hydrogenation reactions over L-$lysine/Ni/Nb_2O_5$

have excellent universality.

L-lysine modification strategy is also applicable on different supports, L-lysine$_{0.05}$/Ni/Nb_2O_5, L-lysine$_{0.05}$/Ni/TiO_2, and L-lysine$_{0.05}$/Ni/Al_2O_3 are prepared by the identical impregnation method and subsequent thermal reduction in H_2. It is obvious that the main product over these catalysts without L-lysine modification is ethylbenzene (Table S3, entries 1-4). The selectivity of styrene can reach around 90% over Ni-based catalysts modulated by L-lysine under light. The L-lysine modification strategy has also been applied to other metals including Pt and Pd for hydrogenation of phenylacetylene. It can be clearly seen that this modification strategy does not regulate the selectivity of styrene (Table S3, entries 5 and 6). These results suggest that L-lysine modification is an effective strategy for Ni-based catalyst in selective phenylacetylene hydrogenation reaction.

Other amino acids are also used to verify whether the selectivity of styrene can be adjusted under visible light irradiation (Table S4). It can be clearly found that glutamylamine, glutamic acid, leucine and glycine modification can also maintain the selectivity of styrene (around 90%). The results confirm that Ni/Nb_2O_5, modified by amino acids with bidentate ligand is beneficial to improve the selectivity of styrene under light irradiation.

4. CONCLUSIONS

L-lysine modified Ni/Nb_2O_5 has been prepared successfully and show excellent photocatalytic performance in the selectivie hydrogenation of phenylacetylene. Metallic Ni is demonstrated to be the active center for phenylacetylene hydrogenation to styrene under visible light irradiation. And there exist strong interaction between both $-COO^-$ and $-NH_2$ groups of L-lysine and Ni/Nb_2O_5 due to N and O coordination, demonstrated by FT-IR, XPS and DFT caculation, leading to high stability of metallic Ni and L-lysine/Ni/Nb_2O_5. High styrene selectivity is because that the styrene has longer distance and lower adsorption energy on the surface of metallic Ni sites than that of phenylacetylene. The enhanced photocatalytic activity of L-lysine/Ni/Nb_2O_5 is mainly attributed to electrons transfer excited by the LSPR effect of Ni NPs under light irradiation and the enriched electrons on the surface of Ni modulated by styrene *in situ*. This L-lysine modification strategy is also suitable for other Ni-based catalysts. In addition, Ni/Nb_2O_5 modified by other amino acids can also increase the selectivity of styrene. This will provide a prospective protocol to increase olefin selectivity in alkyne hydrogenation reaction.

ASSOCIATED CONTENT

Supporting Information

Discussions; additional figures and tables including properties of Ni-based catalysts; structural characterization; models; DFT calculations; additional experimental data; and references.

AUTHOR INFORMATION

Corresponding Authors

Ruiyi Wang — *State Key Laboratory of Coal Conversion, Institute of Coal Chemistry, Taiyuan 030001, China*；E-mail: wangruiyi@sxicc.ac.cn

Xuebin Ke — *Department of Chemical Engineering, University of Hull, HU6 7RX, United Kingdom*；E-mail: x.ke@hull.ac.uk

Guangtao Yu — *Engineering Research Center of Industrial Biocatalysis, Fujian Province University, Fujian Provincial Key Laboratory of Advanced Materials Oriented Chemical Engineering, College of Chemistry and Materials Science, Fujian Normal University, Fuzhou*

350007, China；Fujian Provincial Key Laboratory of Theoretical and Computational Chemistry, Xiamen University, Xiamen, 361005, China； E-mail: yugt@fjnu.edu.cn

Zhanfeng Zheng — *State Key Laboratory of Coal Conversion, Institute of Coal Chemistry, Taiyuan 030001, China；Center of Materials Science and Optoelectronics Engineering, University of Chinese Academy of Sciences, Beijing 100049, China；* E-mail: zfzheng@sxicc.ac.cn

Author Contributions

Jie Wang: data curation, formal analysis, investigation, writing of original draft
Mengxia Wang: theoretical calculation and formal analysis
Linjuan Pei: formal analysis and investigation
Xianmo Gu: validation and formal analysis
Xincheng Li: formal analysis
Peng Kong: formal analysis
Ruiyi Wang: funding acquisition and validation
Xuebin Ke: formal analysis and validation
Guangtao Yu: funding acquisition, project administration, theoretical calculation and validation
Zhanfeng Zheng: funding acquisition, project administration and validation

Notes

The authors declare no competing financial interest.

ACKNOWLEDGMENT

This work was supported by the National Natural Science Foundation of China (22072176, 21773284, 21703276, 21673094, and U1805234),), UK Research and Innovation (UKRI), the Shanxi Science and Technology Department (201801D221093), award foundation for excellent PhD graduates work in Shanxi Province (SQ2019005), the Hundred Talents Program of the Chinese Academy of Sciences and Shanxi Province, and startup fund for high-level talent at Fujian Normal University. We acknowledge the Computing Center of Jilin Province and the High Performance Computing Center (HPCC) of Jilin University for supercomputer time.

REFERENCES

1. Riley, C.; Zhou, S.; Kunwar, D.; De La Riva, A.; Peterson, E.; Payne, R.; Gao, L.; Lin, S.; Guo, H.; Datye, A., Design of effective catalysts for selective alkyne hydrogenation by doping of ceria with a single-atom promotor. *J. Am. Chem. Soc.* **2018,** *140*, 12964-12973.

2. Cao, Y.; Zhang, H.; Ji, S.; Sui, Z.; Jiang, Z.; Wang, D.; Zaera, F.; Zhou, X.; Duan, X.; Li, Y., Adsorption site regulation to guide atomic design of Ni-Ga catalysts for acetylene semi-hydrogenation. *Angew. Chem. Int. Ed.* **2020,** *59*, 11647-11652.

3. Choe, K.; Zheng, F. B.; Wang, H.; Yuan, Y.; Zhao, W. S.; Xue, G. X.; Qiu, X. Y.; Ri, M.; Shi, X. H.; Wang, Y. L.; Li, G. D.; Tang, Z. Y., Fast and selective semihydrogenation of alkynes by palladium nanoparticles sandwiched in metal-organic frameworks. *Angew. Chem. Int. Ed.* **2020,** *59*, 3650-3657.

4. Ryabchuk, P.; Agostini, G.; Pohl, M. M.; Lund, H.; Agapova, A.; Junge, H.; Junge, K.; Beller, M., Intermetallic nickel silicide nanocatalyst-A non-noble metal-based general hydrogenation catalyst. *Sci. Adv.* **2018,** *4*, eaat0761.

5. Wang, Y. L.; Huang, Z. D.; Huang, Z., Catalyst as colour indicator for endpoint detection to enable selective alkyne trans-hydrogenation with ethanol. *Nature Catal.* **2019,** *2*, 529-536.
6. Bu, J.; Liu, Z. P.; Ma, W. X.; Zhang, L.; Wang, T.; Zhang, H. P.; Zhang, Q. Y.; Feng, X. L.; Zhang, J., Selective electrocatalytic semihydrogenation of acetylene impurities for the production of polymer-grade ethylene. *Nat. Catal.* **2021,** *4*, 557-564.
7. Zhou, S.; Shang, L.; Zhao, Y.; Shi, R.; Waterhouse, G. I. N.; Huang, Y. C.; Zheng, L.; Zhang, T., Pd single‐atom catalysts on nitrogen-doped graphene for the highly selective photothermal hydrogenation of acetylene to ethylene. *Adv. Mater.* **2019,** *31,* 1900509.
8. Liu, S. Y.; Niu, Y. M.; Wang, Y. Z.; Chen, J. N.; Quan, X. P.; Zhang, X.; Zhang, B. S., Unravelling the role of active-site isolation in reactivity and reaction pathway control for acetylene hydrogenation. *Chem. Commun.* **2020,** *56*, 6372-6375.
9. Zhang, L.; Zhou, M.; Wang, A.; Zhang, T., Selective hydrogenation over supported metal catalysts: From nanoparticles to single atoms. *Chem. Rev.* **2020,** *120*, 683-733.
10. Wei, Z.; Yao, Z.; Zhou, Q.; Zhuang, G.; Zhong, X.; Deng, S.; Li, X.; Wang, J., Optimizing alkyne hydrogenation performance of Pd on carbon in situ decorated with oxygen-deficient TiO_2 by integrating the reaction and diffusion. *ACS Catal.* **2019,** *9*, 10656-10667.
11. Liang, H.; Zhang, B.; Ge, H.; Gu, X.; Zhang, S.; Qin, Y., Porous TiO_2/Pt/TiO_2 sandwich catalyst for highly selective semihydrogenation of alkyne to olefin. *ACS Catal.* **2017,** *7*, 6567-6572.
12. Bridier, B.; Perez-Ramirez, J., Cooperative effects in ternary Cu-Ni-Fe catalysts lead to enhanced alkene selectivity in alkyne hydrogenation. *J. Am. Chem. Soc.* **2010,** *132*, 4321-4327.
13. Golubina, E. V.; Lokteva, E. S.; Erokhin, A. V.; Veligzhanin, A. A.; Zubavichus, Y. V.; Likholobov, V. A.; Lunin, V. V., The role of metal–support interaction in catalytic activity of nanodiamond-supported nickel in selective phenylacetylene hydrogenation. *J. Catal.* **2016,** *344*, 90-99.
14. Carrara, N.; Betti, C.; Coloma-Pascual, F.; Almansa, M. C.; Gutierrez, L.; Miranda, C.; Quiroga, M. E.; Lederhos, C. R., High-active metallic-activated carbon catalysts for selective hydrogenation. *Int. J. Chem. Eng.* **2018,** *2018*, 1-11.
15. Liu, Y.; Zhao, J.; Feng, J.; He, Y.; Du, Y.; Li, D., Layered double hydroxide-derived Ni-Cu nanoalloy catalysts for semi-hydrogenation of alkynes: Improvement of selectivity and anti-coking ability via alloying of Ni and Cu. *J. Catal.* **2018,** *359*, 251-260.
16. Yu, J. W.; Wang, X. Y.; Yuan, C. Y.; Li, W. Z.; Wang, Y. H.; Zhang, Y. W., Synthesis of ultrathin Ni nanosheets for semihydrogenation of phenylacetylene to styrene under mild conditions. *Nanoscale* **2018,** *10*, 6936-6944.
17. Long, Y.; Li, J.; Wu, L.; Wang, Q.; Liu, Y.; Wang, X.; Song, S.; Zhang, H., Construction of trace silver modified core@shell structured Pt-Ni nanoframe@CeO_2 for semihydrogenation of phenylacetylene. *Nano Res.* **2019,** *12*, 869-875.
18. Murugesan, K.; Bheeter, C. B.; Linnebank, P. R.; Spannenberg, A.; Reek, J. N. H.; Jagadeesh, R. V.; Beller, M., Nickel-catalyzed stereodivergent synthesis of *E*- and *Z*-Alkenes by hydrogenation of alkynes. *ChemSusChem* **2019,** *12*, 3363-3369.
19. Rath, P. C.; Mishra, M.; Saikia, D.; Chang, J. K.; Perng, T.-P.; Kao, H.-M., Facile fabrication of titania-ordered cubic mesoporous carbon composite: Effect of Ni doping on photocatalytic hydrogen generation. *Int. J. Hydrogen Energ.* **2019,** *44*, 19255-19266.

20. Li, C.; Chen, Y.; Zhang, S.; Zhou, J.; Wang, F.; He, S.; Wei, M.; Evans, D. G.; Duan, X., Nickel-gallium intermetallic nanocrystal catalysts in the semihydrogenation of phenylacetylene. *ChemCatChem* **2014,** *6*, 824-831.

21. Cao, Y.; Zhang, H.; Ji, S.; Sui, Z.; Jiang, Z.; Wang, D.; Zaera, F.; Zhou, X.; Duan, X.; Li, Y., Adsorption site regulation to guide atomic design of Ni-Ga catalysts for acetylene semi-hydrogenation. *Angew. Chem. Int. Ed.* **2020,** *59*, 11647-11652.

22. Yang, L.; Yu, S.; Peng, C.; Fang, X.; Cheng, Z.; Zhou, Z., Semihydrogenation of phenylacetylene over nonprecious Ni-based catalysts supported on AlSBA-15. *J. Catal.* **2019,** *370*, 310-320.

23. Niu, Y.; Huang, X.; Wang, Y.; Xu, M.; Chen, J.; Xu, S.; Willinger, M. G.; Zhang, W.; Wei, M.; Zhang, B., Manipulating interstitial carbon atoms in the nickel octahedral site for highly efficient hydrogenation of alkyne. *Nat. Commun.* **2020,** *11*, 3324.

24. Shi, X.; Wen, X.; Nie, S.; Dong, J.; Li, J.; Shi, Y.; Zhang, H.; Bai, G., Fabrication of Ni_3N nanorods anchored on N-doped carbon for selective semi-hydrogenation of alkynes. *J. Catal.* **2020,** *382*, 22-30.

25. Kwon, S. G.; Krylova, G.; Sumer, A.; Schwartz, M. M.; Bunel, E. E.; Marshall, C. L.; Chattopadhyay, S.; Lee, B.; Jellinek, J.; Shevchenko, E. V., Capping ligands as selectivity switchers in hydrogenation reactions. *Nano Lett.* **2012,** *12*, 5382-5388.

26. López-Vinasco, A. M.; Martínez-Prieto, L. M.; Asensio, J. M.; Lecante, P.; Chaudret, B.; Cámpora, J.; van Leeuwen, P. W. N. M., Novel nickel nanoparticles stabilized by imidazolium-amidinate ligands for selective hydrogenation of alkynes. *Catal. Sci. Technol.* **2020,** *10*, 342-350.

27. Rai, R. K.; Awasthi, M. K.; Singh, V. K.; Barman, S. R.; Behrens, S.; Singh, S. K., Aqueous phase semihydrogenation of alkynes over Ni–Fe bimetallic catalysts. *Catal. Sci. Technol.* **2020,** *10*, 4968-4980.

28. Mateo, D.; Morlanes, N.; Maity, P.; Shterk, G.; Mohammed, O. F.; Gascon, J., Efficient visible-light driven photothermal conversion of CO_2 to methane by nickel nanoparticles supported on barium titanate. *Adv. Funct. Mater.* **2020**, 2008244.

29. Liu, H.; Dao, T. D.; Liu, L.; Meng, X.; Nagao, T.; Ye, J., Light assisted CO_2 reduction with methane over group VIII metals: Universality of metal localized surface plasmon resonance in reactant activation. *Appl. Catal., B* **2017,** *209*, 183-189.

30. Zhang, Y.; Pei, L.; Zheng, Z.; Yuan, Y.; Xie, T.; Yang, J.; Chen, S.; Wang, J.; Waclawik, E. R.; Zhu, H., Heterojunctions between amorphous and crystalline niobium oxide with enhanced photoactivity for selective aerobic oxidation of benzylamine to imine under visible light. *J. Mater. Chem. A* **2015,** *3*, 18045-18052.

31. Zhu, H. Y.; Zheng, Z. F.; Gao, X. P.; Huang, Y. N.; Yan, Z. M.; Zou, J.; Yin, H. M.; Zou, Q. D.; Kable, S. H.; Zhao, J. C.; Xi, Y. F.; Martens, W. N.; Frost, R. L., Structural evolution in a hydrothermal reaction between Nb_2O_5 and NaOH solution: From Nb_2O_5 grains to microporous $Na_2Nb_2O_6{\cdot}2/3H_2O$ fibers and $NaNbO_3$ cubes. *J. Am. Chem. Soc.* **2006,** *128*, 2373-2384.

32. Wang, J.; Gu, X.; Pei, L.; Kong, P.; Zhang, J.; Wang, X.; Wang, R.; Waclawik, E. R.; Zheng, Z., Strong metal-support interaction induced O_2 activation over Au/MNb_2O_6 ($M = Zn^{2+}$, Ni^{2+} and Co^{2+}) for efficient photocatalytic benzyl alcohol oxidative esterification. *Appl. Catal., B* **2021,** *283*, 119618.

33. Becke, A. D., A new mixing of Hartree-Fock and local density-functional theories. *J. Chem. Phys.* **1993,** *98*, 1372-1377.

34. Kresse, G.; Hafner, J., Ab initio molecular dynamics for liquid metals. *Phys. Review B* **1993,** *47*, 558-561.

35. Kresse, G.; Hafner, J., Ab initio molecular-dynamics simulation of the liquid-metal–amorphous-semiconductor transition in germanium. *Phys. Review B* **1994,** *49*, 14251-14269.
36. Wu, X.; Vargas, M. C.; Nayak, S.; Lotrich, V.; Scoles, G., Towards extending the applicability of density functional theory to weakly bound systems. *J. Chem. Phys.* **2001,** *115*, 8748-8757.
37. Blöchl, P. E., Projector augmented-wave method. *Phys. Review B* **1994,** *50*, 17953-17979.
38. Kresse, G.; Joubert, D., From ultrasoft pseudopotentials to the projector augmented-wave method. *Phys. Review B* **1999,** *59*, 1758-1775.
39. Wilson, K. E.; Baddeley, C. J., Chiral assemblies of nickel lysinate via the corrosive adsorption of (S)-lysine on Ni/Au{111}. *Surf. Sci.* **2014,** *629*, 102-107.
40. Humblot, V.; Methivier, C.; Pradier, C. M., Adsorption of L-lysine on Cu(110): A RAIRS study from UHV to the liquid phase. *Langmuir* **2006,** *22*, 3089-3096.
41. Mateo, D.; Albero, J.; García, H., Graphene supported NiO/Ni nanoparticles as efficient photocatalyst for gas phase CO_2 reduction with hydrogen. *Appl. Catal., B* **2018,** *224*, 563-571.
42. Li, S.; Wang, L.; Li, Y.; Zhang, L.; Wang, A.; Xiao, N.; Gao, Y.; Li, N.; Song, W.; Ge, L.; Liu, J., Novel photocatalyst incorporating Ni-Co layered double hydroxides with P-doped CdS for enhancing photocatalytic activity towards hydrogen evolution. *Appl. Catal., B* **2019,** *254*, 145-155.
43. Ni, J.; Leng, W.; Mao, J.; Wang, J.; Lin, J.; Jiang, D.; Li, X., Tuning electron density of metal nickel by support defects in Ni/ZrO_2 for selective hydrogenation of fatty acids to alkanes and alcohols. *Appl. Catal., B* **2019,** *253*, 170-178.
44. Yang, Y.; Sun, X.; Han, G.; Liu, X.; Zhang, X.; Sun, Y.; Zhang, M.; Cao, Z.; Sun, Y., Enhanced electrocatalytic hydrogen oxidation on Ni/NiO/C derived from a nickel-based metal-organic framework. *Angew. Chem. Int. Ed.* **2019,** *58*, 10644-10649.
45. Merlin, N.; Nogueira, B. A.; de Lima, V. A.; dos Santos, L. M., Application of Fourier transform infrared spectroscopy, chemical and chemometrics analyses to the characterization of agro-industrial waste. *Quim. Nova.* **2014,** *37*, 1584-1588.
46. Ramya, K.; Saraswathi, N. T.; Raja, C. R., Growth and characterization of L-Lysine adipate crystal. *Optics & Laser Technol.* **2017,** *90*, 222-225.
47. Wang, X. Y.; Wang, R. Y.; Gu, X. M.; Jia, J. F.; Zheng, Z. F., Light-assisted O-methylation of phenol with dimethyl carbonate over a layered double oxide catalyst. *Catal. Sci. Technol.* **2019,** *9*, 1774-1778.
48. Zhang, X.; Ke, X.; Zhu, H., Zeolite-supported gold nanoparticles for selective photooxidation of aromatic alcohols under visible-light irradiation. *Chem. Eur. J.* **2012,** *18*, 8048-8056.
49. Sarina, S.; Waclawik, E. R.; Zhu, H., Photocatalysis on supported gold and silver nanoparticles under ultraviolet and visible light irradiation. *Green Chem.* **2013,** *15*, 1814-1833.
50. Xiao, Q.; Sarina, S.; Jaatinen, E.; Jia, J. F.; Arnold, D. P.; Liu, H. W.; Zhu, H. Y., Efficient photocatalytic Suzuki cross-coupling reactions on Au-Pd alloy nanoparticles under visible light irradiation. *Green Chem.* **2014,** *16*, 4272-4285.
51. Xiao, Q.; Liu, Z.; Bo, A.; Zavahir, S.; Sarina, S.; Bottle, S.; Riches, J. D.; Zhu, H., Catalytic transformation of aliphatic alcohols to corresponding esters in O_2 under neutral conditions using visible-light irradiation. *J. Am. Chem. Soc.* **2015,** *137*, 1956-1966.
52. Xiong, Z.; Chen, X.; Wang, X.; Peng, L.; Yan, D.; Lei, H.; Fu, Y.; Wu, J.; Li, Z.; An, X.; Wu, W., Size dependence of plasmon absorption of Ni nanoparticles embedded in $BaTiO_3$/$SrTiO_3$ superlattices. *Appl. Surf. Sci.* **2013,** *268*, 524-528.

53. Solis-Garcia, A.; Louvier-Hernandez, J. F.; Almendarez-Camarillo, A.; Fierro-Gonzalez, J. C., Participation of surface bicarbonate, formate and methoxy species in the carbon dioxide methanation catalyzed by ZrO_2-supported Ni. *Appl. Catal., B* **2017,** *218*, 611-620.